

Implications of HERA measurements for LHC*

M. Diehl

Deutsches Elektronen-Synchrotron DESY, 22603 Hamburg, Germany

Abstract: I discuss the theoretical understanding of key measurements at HERA and their relevance for physics at LHC, focusing on recent developments for structure functions and for diffraction.

1 Introduction

In this talk I discuss key measurements at HERA and their impact on physics at LHC, focusing on the topics of structure functions and of diffraction. Many important features of the final state such as jets, multiple interactions, etc. will not be covered for lack of time. A wealth of up-to-date information can be found in the presentations of the Workshop on HERA and the LHC [1].

2 Structure functions

A fundamental observable in deep inelastic scattering (DIS) is the structure function F_2 of the proton. A chief discovery of HERA is its rapid rise with increasing energy or decreasing Bjorken- x , shown in Fig. 1. This has triggered many theory developments, which continue to provide insight into the dynamics of QCD at high energies. In addition, the wide kinematic range and high precision of the HERA structure function data makes them a key input to the determination of parton densities (PDFs), which are in particular needed to calculate the effective luminosities of colliding partons at LHC. The increasing precision of HERA data has been matched by theoretical calculations up to next-to-next-to-leading order (NNLO) in α_s [3].

An example of a process where high precision is needed at LHC is the production of a weak gauge boson, W or Z , which has been proposed as a possible luminosity monitor. Fig. 2 shows the corresponding cross sections calculated with different recent sets of PDFs. The error bars on the cross sections reflect the errors provided in the PDF parameterizations. It is important to keep in mind that they quantify the errors on the data to which the PDFs have been fitted, but not uncertainties due to the choice of parameterization, details of the theory description, or the data selection. As is clear from the figure, one can be misled when taking the errors in a given PDF parameterization as a measure for the actual uncertainty on the parton densities. The same conclusion has been obtained in an earlier study of Higgs production [5], which is one of the prime signal channels at LHC. An illustration of how much even the most recent PDF extractions can differ is given in Fig. 3, which shows the gluon distribution obtained in the studies [6] and [7], both of which describe DIS at NNLO. The shape of the distribution is drastically different in the two analyses, and below $x = 10^{-2}$ their respective error bands do not overlap.

2.1 Heavy flavor production

The most important observable for determining the gluon density at small x is the scaling violation in the structure function $F_2(x, Q^2)$. Because of cross talk between gluons and sea

*Talk presented at the XXIII International Symposium on Lepton and Photon Interactions at High Energy (LP07), Daegu, Korea, 13–18 August 2007

HERA I e^+p Neutral Current Scattering - H1 and ZEUS

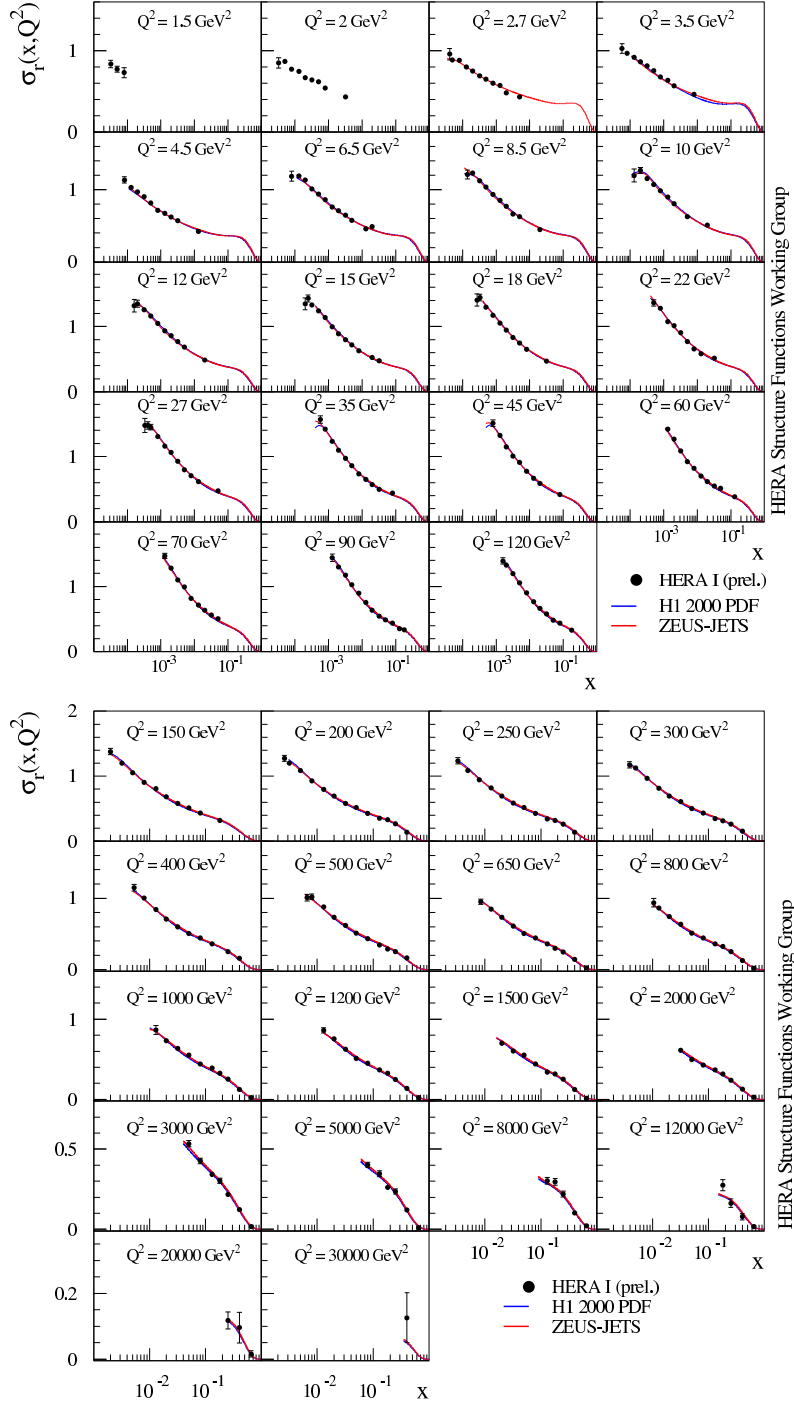


Figure 1: HERA data for inclusive deep inelastic scattering [2]. When neglecting Z exchange and the longitudinal structure function F_L , the reduced cross section is $\sigma_r \approx F_2(x, Q^2)$.

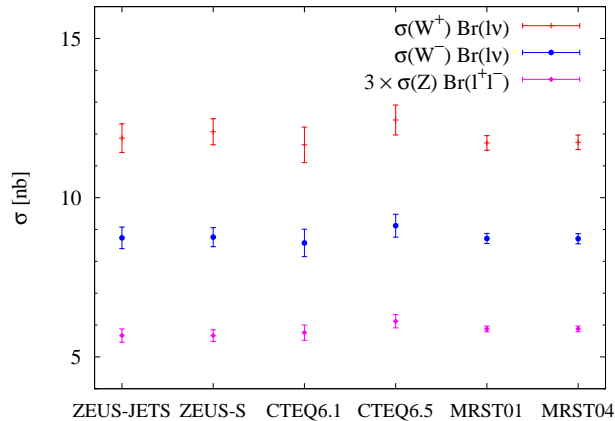


Figure 2: Cross sections for W and Z production with leptonic decay at LHC, calculated with different sets of PDFs and their error estimates. The numbers have been taken from Table 1 in [4] and correspond to the full rapidity range of the produced gauge boson.

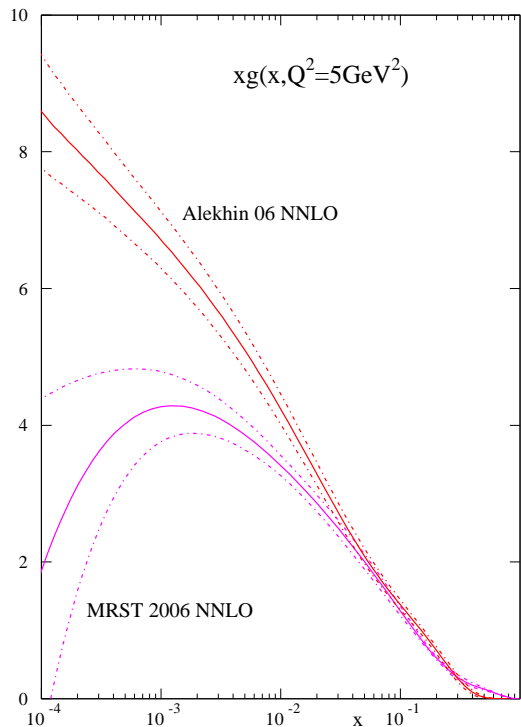


Figure 3: Gluon distributions including error bands from two recent analyses [6, 7]. The figure is taken from [6].

quarks in the Q^2 evolution, this leaves however room for ambiguities such as the one in Fig. 3. An observable that may provide independent constraints is the structure function F_2^c for inclusive charm production. Several schemes can be used to describe charm production in ep or pp collisions:

- The fixed flavor number scheme (FFNS) treats only the light quark flavors u , d , s as partons and calculates the production of charm from the splitting $g \rightarrow c\bar{c}$ at fixed order in α_s . Most suitable when the hard scale Q^2 in the process is comparable to m_c^2 , this scheme turns out to work rather well in most of the relevant kinematics for F_2^c at HERA. At very high scales, it is bound to fail because it misses large logarithms $\alpha_s^n \log^n(Q^2/m_c^2)$ from higher orders.
- In the zero-mass variable flavor number scheme (ZM-VFNS), charm is treated as a massless parton, so that the logarithms just mentioned are resummed to all orders by the evolution of the parton densities. Such a scheme is adequate for charm production at high transverse momenta at HERA, Tevatron, and especially at LHC, where important signal channels contain charm in the final state. Neglecting the charm quark mass, this scheme is however inadequate for describing data with $Q^2 \sim m_c^2$.
- General-mass variable flavor number

schemes (GM-VFNS) have been devised to interpolate smoothly between the two extremes just described. Progress has recently been made on nontrivial issues that arise when consistently matching the descriptions with n_f and $n_f + 1$ light quark flavors, see e.g. [8, 9].

An analogous discussion holds for the production of bottom quarks. Here again, it is only an interpolating scheme that can simultaneously use input from the bottom structure function F_2^b at HERA and provide b quark PDFs for calculating the production of bottom quarks with high transverse momentum at LHC. In a recent review [10], HERA data for F_2^c and F_2^b are compared with calculations using different schemes. With further data from run II of HERA, experimental errors are expected to decrease significantly, and heavy flavor structure functions should provide stringent tests of the theory description and the gluon density.

2.2 Recent parton density fits

The progress in the determination of PDFs is documented in a number of recent fits, of which I can only mention a few:

- The MRST 2006 parton set [6] updates previous analyses by the MRST group. It is a global fit to data for numerous processes, with inclusive DIS and Drell-Yan lepton pair production calculated at NNLO (other processes like jet production are only available at NLO). Improvements in describing the charm and bottom contributions to F_2 at NNLO have led to significant changes compared with the MRST 2004 partons. These changes increase the W and Z production cross sections at LHC by about 6%.
- The CTEQ6.5 partons [11, 12] are obtained from a global fit to data using NLO theory. Significant changes are obtained compared with the previous CTEQ6.1 set, which used a ZM-VFNS whereas the new fit employs a GM-VFNS, which is much more adequate for describing the heavy flavor part

of the HERA structure functions. The influence of these changes on key processes at LHC is clearly seen in Fig. 2.

- The Alekhin 06 parameterization [7] is obtained from only DIS and Drell-Yan data, which allows one to use NNLO accuracy throughout. The heavy-flavor contributions to F_2 are treated at order α_s^2 in the FFNS with $n_f = 3$.
- The analysis in [13] is restricted to DIS data and to non-singlet combinations of PDFs. This avoids uncertainties on the gluon density and allows for fits at NNLO and NNNLO accuracy.

Apart from extracting parton densities, such analyses also permit an extraction of the strong coupling constant α_s , whose precision has become very competitive with other determinations, see [13, 14]. In this field, HERA contributes both with DIS structure functions in a wide range of Q^2 and with dedicated analyses of jet production [15].

2.3 High Q^2

For separating the densities of different quarks and antiquarks, crucial information comes from experiments other than HERA. In particular, Drell-Yan lepton pairs and W^\pm production at the Tevatron [16] provide a handle for the separation of \bar{u} and \bar{d} distributions, whereas data from DIS experiments with ν and $\bar{\nu}$ beams give the strongest constraints on s and \bar{s} distributions [11]. Nevertheless, structure function data from HERA contribute to this field as well, in particular in the large Q^2 region, where Z or W exchange becomes measurable. The theoretical interpretation of such data is very clean, since there are no nuclear corrections and since inclusive DIS can be analyzed at NNLO. Important observables are the structure functions for the interference of γ and Z exchange: the lepton beam charge asymmetry gives access to $F_3^{\gamma Z}$, which permits a clean measurement of the valence quark combinations $q - \bar{q}$, and $F_2^{\gamma Z}$ from the lepton beam polarization asymmetry is sensitive to the flavor combination $u + d$.

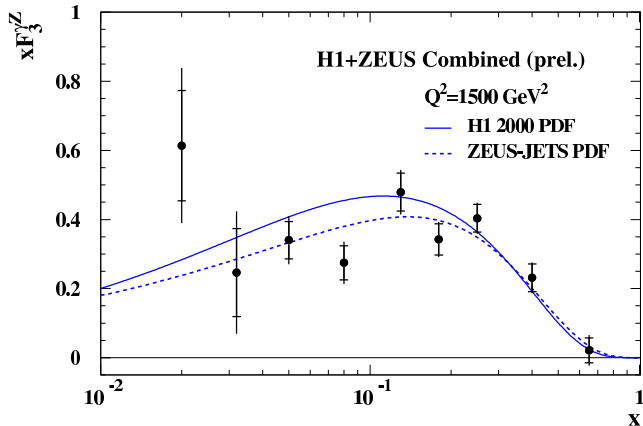


Figure 4: HERA results for the structure function $F_3^{\gamma Z}$, which describes the interference of γ and Z exchange [17]. The data shown in this plot correspond to about half of the full HERA statistics.

Results for $F_3^{\gamma Z}$ are shown in Fig. 4. Charged current DIS in e^+p involves the combinations $u+c$ and $\bar{d}+\bar{s}$, whereas its counterpart in e^-p involves $\bar{u}+\bar{c}$ and $d+s$. It will be interesting to see whether a selective measurement of the strange quark distribution by tagging charm in the final state is practically feasible. In all measurements just mentioned, the size of experimental errors is crucial, and one will have to wait for the analysis of the full HERA data set to assess their impact on the precision of PDFs for different quark and antiquark flavors. Such detailed knowledge becomes important in flavor sensitive new-physics channels at LHC, as has been illustrated in [11] for the example of charged Higgs production via $\bar{s}+c \rightarrow H^+$.

2.4 Small x : higher orders

It has long been known that higher perturbative orders play an increasingly important role as x becomes small. This is for instance illustrated by the drastic differences between the gluon densities extracted from DIS data at LO, NLO, and NNLO accuracy. These differences propagate to observables, notably to the structure function $F_L(x, Q^2)$ for longitudinal photon polarization, see e.g. [18]. The reason for these effects are large logarithms $\alpha_s^{n+m} \log^n(1/x)$ in the hard-scattering coefficients and the evolution kernels for the parton densities. It is an ongoing program to sum these logarithms to all orders using the BFKL formalism, see e.g. [19, 20, 21]. Projecting out

the leading-twist part, i.e. the leading terms in $1/Q^2$, opens the possibility to combine the resummed results at small x with the fixed-order ones at higher x . The state-of-the-art is next-to-leading logarithmic accuracy, where terms $\alpha_s^{n+m} \log^n(1/x)$ with $m = 0, 1$ are resummed, and progress has recently been made on difficult technical issues such as the treatment of the running coupling and the inclusion of quarks. A first application in a global parton density fit has been presented in [20], with a very clear impact of resummation on both the gluon density and on F_L . It will be interesting to see the further development of these efforts.

The longitudinal structure function F_L is a basic observable in DIS, at par with the well-measured structure function F_2 . Starting at order α_s , it is more directly sensitive to the gluon distribution than F_2 , and not surprisingly it turns out to discriminate strongly between different theoretical treatments of the gluon sector. The low- and medium-energy runs of HERA in the last months of its operation permit a direct measurement of F_L by Rosenbluth separation. This will provide data in a region of moderate Q^2 and small x where the studies just mention show indeed striking differences for various theory inputs.

2.5 Small x : nonlinear effects

So far we have discussed deep inelastic scattering in terms of the leading-twist approximation, which is based on the limit of large Q^2

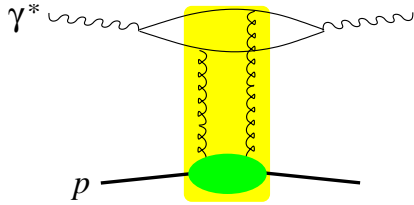


Figure 5: The forward γ^*p amplitude in the color dipole picture. Its imaginary part gives the total γ^*p cross section via the optical theorem. The large shaded (yellow) box represents the dipole scattering amplitude $N_{q\bar{q}}$, and the lower (green) blob stands for the gluon distribution.

and involves perturbatively calculable hard-scattering kernels and parton distributions that evolve according to the DGLAP equations. DGLAP evolution in particular describes the splitting process $g \rightarrow gg$, in which gluons lose momentum, and which leads to a rapidly growing gluon density at small x . The transverse “size” of a gluon as it is resolved in a hard process is given by the inverse $1/Q$ of the large momentum scale. When $g(x, Q^2)$ is so large that gluons overlap in transverse space, they will recombine into gluons with larger momentum, so that the growth of the density will be slowed down and eventually saturate. The region in x and Q^2 where such nonlinear effects become important is delineated by the saturation scale $Q_s^2(x)$, which is a decreasing function of x .

There are vigorous theoretical activities to describe this nonlinear dynamics at various degrees of approximation. I cannot describe them within the limitations of this talk, and only mention keywords like the Balitsky-Kovchegov equation, the JIMWLK equation, and pomeron loops. A recent overview and references can be found in [22]. At the phenomenological level, nonlinear effects in a large class of DIS processes can be described using the color-dipole formulation. Its basic ingredient is the amplitude $N_{q\bar{q}}$ for the scattering of a quark-antiquark dipole on a proton target, as shown in Fig. 5. In the kinematic region where nonlinear effects are unimpor-

tant, $N_{q\bar{q}}$ is related to the gluon density, so that one can make contact with the leading-twist description. Several studies have proposed phenomenological parameterizations of $N_{q\bar{q}}$ with saturation behavior due to nonlinear effects, and fitted them to DIS data from HERA. This gives a good description of F_2 at small x , down to Q^2 much below the values where the leading-twist description is applicable. More recently, due attention has also been paid to the charm contribution F_2^c , where good agreement with the data is achieved as well [23, 24, 25]. This description gains much credibility from the fact that with the same nonperturbative input one can describe several diffractive processes, as I will discuss in Section 3. The saturation mechanism predicts geometric scaling, which states that F_2 at small x depends on x and Q^2 only in the combination $Q^2/Q_s^2(x)$. This scaling is indeed seen in HERA data, and I refer to [26] for a recent critical discussion and references. Taken together, these features can be seen as strong indications that nonlinear effects are at work in the small- x region at HERA, although there is no unambiguous proof of this so far. It should also be mentioned that the treatment of higher perturbative orders in the theory of nonlinear effects is more difficult and much less advanced than in the leading-twist approximation.

Table 1 compares the saturation scales obtained in recent phenomenological analyses. For $x = 10^{-4}$, which is a typical value for HERA, one finds Q_s slightly below 1 GeV. This is at the borderline of applicability for QCD perturbation theory, which is part of the difficulty to prove or disprove the valid-

Table 1: The saturation scale $Q_s(x)$ obtained by recent analyses of HERA data in the dipole approach.

$x = 10^{-4}$	$x = 10^{-6}$	Reference
0.8 GeV	4.0 GeV	[23]
0.8 GeV	2.0 GeV	[24]
0.7 GeV	1.9 GeV	[25]

ity of the theoretical approach in the HERA regime. The spread in Q_s at $x = 10^{-6}$ is hardly surprising and indicates the theoretical uncertainties involved in such an extrapolation. HERA measurements have driven many efforts to quantify the onset of nonlinear effects in hard scattering at high energy. With detectors for very forward particles at LHC, there is the prospect of pursuing such studies in pp collisions. It has for instance been estimated [27] that one can detect Drell-Yan lepton pairs with $x \lesssim 10^{-6}$ and invariant mass $Q^2 \gtrsim 4 \text{ GeV}^2$ using the CASTOR calorimeter. According to Table 1, nonlinear effects may well be strong in that region. The study of saturation effects at HERA has also helped in developing a quantitative description of the initial state in heavy-ion collisions, presently at RHIC and soon at ALICE, see e.g. [28].

Expanding the DIS cross section obtained in the dipole approach in powers of $1/Q^2$, one can isolate the leading term, which corresponds to what is described by the leading-twist approach. An early study in [29] found for the ratio of the full result and its twist-two approximation

$$\frac{F_2^{\text{full}}}{F_2^{t=2}} \approx 0.94, \quad \frac{F_L^{\text{full}}}{F_L^{t=2}} \approx 0.66 \quad (1)$$

at $Q^2 = 5 \text{ GeV}^2$ and $x = 2.5 \times 10^{-4}$, which is a typical point in HERA kinematics. We see that the longitudinal structure function is much more affected than F_2 by nonlinear effects, which highlights once more the dynamical sensitivity of this observable. Unfortunately, the numbers in eq. (1) are based on a fairly old parameterization of the dipole scattering amplitude. An update of such a study for more recent models would be useful, since a result as in eq. (1) would have important consequences on the theoretical error one should assign to extractions of PDFs using the leading-twist approximation of F_2 .

3 Diffraction

A striking discovery of HERA is that a large fraction (around 10%) of events in DIS have a leading proton or a large rapidity gap between

the proton remnant and the other hadrons in the final state. The increasing precision and kinematic coverage of the data [30, 31] reveals in particular two crucial features of the cross section for inclusive diffraction, $\gamma^*p \rightarrow X + p$.

- The ratio $\sigma_{\text{diff}}/\sigma_{\text{tot}}$ of the diffractive and the total γ^*p cross sections is rather flat in Q^2 for fixed x (except in corners of phase space). This means that inclusive diffraction is a leading-twist phenomenon in γ^*p interactions and gives a significant contribution to the inclusive structure function F_2 at high Q^2 .

This observation contains an important general lesson. There is no doubt that the leading-twist description of the *inclusive* γ^*p cross section is adequate at high Q^2 : it is based on factorization theorems in QCD and works to high precision in practice. This does however not imply that the same type of leading-twist description, together with standard hadronization models as they are implemented in event generators, gives an adequate description of the *final state*. Such a description fails to account for the large observed fraction of rapidity gap events. From the theory side this not surprising: the derivation of factorization theorems for inclusive observables heavily relies on taking a *sum* over final states.

- At given Q^2 the cross section ratio $\sigma_{\text{diff}}/\sigma_{\text{tot}}$ has a very flat dependence on the collision energy, or equivalently on x . As indicated in Fig. 6, both cross sections can be calculated in the dipole approach. The saturation mechanism discussed in Section 2.5 provides a natural explanation of this surprising result, which can be understood using simple analytical approximations and is numerically seen to high precision [32]. It should be mentioned that in a restricted kinematic region, models where the dipole scattering amplitude does not exhibit saturation can also describe the data [33]. This underscores the importance of having precise measurements in a wide kinematic region.

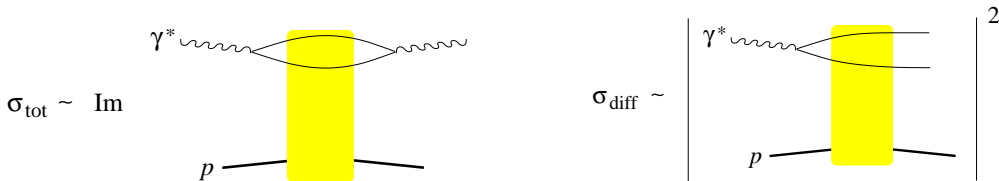


Figure 6: Description of the total and of the diffractive γ^*p cross section in the dipole approach at lowest order in α_s . The shaded (yellow) boxes represent the dipole scattering amplitude.

Compared with inclusive diffraction, the cross sections for exclusive diffractive channels such as vector meson production ($\gamma^*p \rightarrow Vp$) or virtual Compton scattering ($\gamma^*p \rightarrow \gamma p$) at high Q^2 grow significantly faster with energy. This can be understood generically in the saturation approach, and dipole models such as the one in [23] provide a good quantitative description of these channels as well. The relevant graph for $\gamma^*p \rightarrow \gamma p$ has the same form as in Fig. 5. In the region of large Q^2 , where nonlinear effects are negligible, these exclusive processes also admit a leading-twist description, where the gluon density appearing in inclusive processes is replaced by the generalized gluon distribution, which depends on the difference of proton momenta in the initial and final state. Its dependence on the invariant momentum transfer t contains information about the spatial distribution of gluons in the impact parameter plane, whereas x determines the relevant longitudinal momentum fractions [34]. Exclusive diffractive processes thus open the possibility to obtain a three-dimensional picture of how gluons and sea quarks are distributed in the proton. A recent quantitative study can be found in [35], and the relevance of such information for physics at LHC has been discussed in [36].

3.1 pp and $p\bar{p}$ collisions

A key for the successful QCD description of diffraction at HERA is that the presence of a hard scale such as Q^2 allows us to calculate part of the process in perturbation theory. It is natural to attempt the same in diffractive processes at pp and $p\bar{p}$ colliders. The CDF Collaboration has studied a number of channels with a leading antiproton or a large ra-

pidity gap, and with a hard scale in the final state provided e.g. by jets, weak gauge bosons or heavy quarks [37]. The fraction of rapidity gaps in such hard processes is found to be at the percent level, about an order of magnitude smaller than the fraction of rapidity gaps in DIS. If one assumes factorization and calculates e.g. diffractive jet production, $p\bar{p} \rightarrow \text{dijet} + X + \bar{p}$ in terms of diffractive parton densities extracted from HERA DIS data, one obtains a rate substantially larger than what is measured [38]. This indicates that in diffractive $p\bar{p}$ and pp interactions, factorization into parton densities and a partonic hard-scattering subprocess is strongly broken. The analysis of factorization proofs indeed shows that interactions between the spectator partons of both hadrons cannot be neglected in such a situation: their effects only cancel in sufficiently *inclusive* observables, where no rapidity gap is required [39]. Such interactions “bypass” the hard scattering and are at least partly soft, so that one has to resort to phenomenological models in order to describe their effect. The combination of diffractive data from HERA and the Tevatron allows one to test such models.

Spectator interactions can also populate the final state with additional particles and thus destroy any rapidity gap, as shown in Fig. 7. There is hence a link between the suppression of hard diffraction and the physics of multiple interactions and the underlying event. The latter is expected to be of great importance at LHC, given the huge phase space available for producing energetic particles by secondary interactions in a single pp collision.

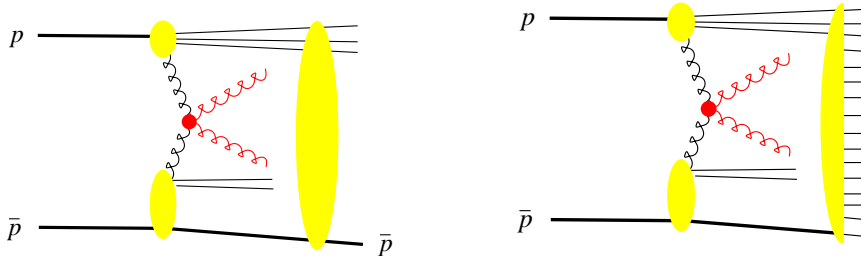


Figure 7: Left: Dijet production with a leading antiproton, $p\bar{p} \rightarrow \text{dijet} + X + \bar{p}$. The small upper blob represents the usual gluon density, the small lower blob stands for the diffractive gluon density, and the large blob denotes interactions between spectator partons in the proton and antiproton. Right: The same type of spectator interactions can populate the final state with particles, thus destroying the rapidity gap.

3.2 Exclusive diffraction at LHC

A particular type of diffractive events at LHC has received considerable attention. If both protons are scattered diffractively, one can produce new particles like the Higgs in a very clean environment, $pp \rightarrow p + H + p$. The same holds for any other particle with a sufficiently large coupling to two gluons. To measure such events is an experimental challenge, requiring very forward detectors and having to overcome relatively low rates and trigger issues, and there are ongoing efforts to achieve this goal [40, 27]. Advantages of exclusive production are the possibility to measure mass and width to an accuracy of a few GeV, the determination of quantum numbers (since $CP = ++$ states are strongly enhanced by the production mechanism), and a generally very favorable signal-to-background ratio. The calculation of the cross section is nontrivial and involves a number of ingredients. Among these are in particular the generalized gluon distribution, which can be extracted from exclusive diffractive channels at HERA, radiative corrections in the form of Sudakov factors, as well as spectator interactions as discussed in the previous subsection. A simplified graph is shown in Fig. 8. Corresponding theoretical calculations are in fair agreement with measurements of similar exclusive channels at the Tevatron, such as dijet or $\gamma\gamma$ production [41].

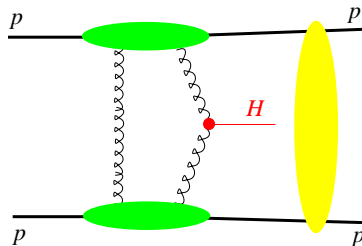


Figure 8: Schematic representation of exclusive Higgs production, $pp \rightarrow p + H + p$. The smaller (green) blobs represent the generalized gluon distribution, and the larger (yellow) one stands for spectator interactions.

Detailed experimental studies have been performed for the production of a light standard model Higgs in the decay channel $H \rightarrow W^+W^-$, with one W being off-shell for $m_H < 2m_W$. For an integrated luminosity of 30 fb^{-1} , a few signal events after triggers and cuts are expected according to [42], with a very low background. The decay channel $H \rightarrow b\bar{b}$ is more difficult experimentally, and for a standard model Higgs it will probably yield too few events after triggers and cuts [43]. In a number of supersymmetric scenarios, however, the production rate is significantly enhanced, especially for large $\tan\beta$. In such cases, exclusive Higgs production in $pp \rightarrow p + b\bar{b} + p$ may be measurable with 3σ significance, and in certain scenarios a 5σ dis-

covery may even be possible with sufficient and moderate Q^2 .
running time [43, 44].

4 Conclusions

HERA has pioneered the study of deep inelastic scattering at small Bjorken- x and at large Q^2 . The kinematic coverage and precision of the data for the inclusive structure function $F_2(x, Q^2)$ provides a key input for the precise determination of parton densities, which is a crucial prerequisite for calculating precise cross sections at LHC. The continuous improvement of the data has been accompanied by substantial progress in the understanding of QCD dynamics at high energy, from the calculation of perturbative corrections and their resummation to the development of a theory for nonlinear effects at very small x .

Diffraction in DIS exhibits a number of simple features, and at the same time shows the intricacies of describing final states in QCD, having invalidated a number of (too) naive expectations. Comparison of diffractive measurements at HERA and the Tevatron reveals the yet higher complexity of the final state in hadron-hadron collisions. Calculations based on these measurements can be used to estimate the exclusive diffractive production of the Higgs and other new particles at LHC. While their detection requires a substantial experimental effort, these clean final states can provide a valuable tool for precise measurements in the Higgs sector, and in some scenarios of physics beyond the Standard Model may even become a discovery channel.

Important results can be expected from the final analysis of the data of HERA run II, since statistics and kinematic reach are still limiting factors in important measurements, such as DIS at high Q^2 , the production of heavy flavors, or various diffractive channels. The direct measurement of the longitudinal structure function F_L will provide a missing cornerstone in the description of inclusive DIS and a sharp discriminator between theoretical approaches to QCD at small x

Acknowledgments

I wish to thank D. Son and his colleagues for organizing a wonderful conference. It is a pleasure to thank H. Abramowicz, J. Bartels, O. Behnke, A. Cooper-Sarkar, L. Dixon, C. Gwenlan, H. Jung, M. Klein, G. Kramer, S. Moch and L. Motyka for discussions and valuable input. Special thanks go to J. Bartels for a careful reading of the manuscript.

References

- [1] <http://www.desy.de/~heralhc>
- [2] H1 and ZEUS Collaborations, report no. H1prelim-07-007 and ZEUS-prel-07-026 prepared for this conference, <https://www-h1.desy.de/publications/H1preliminary.short.list.html>
- [3] S. Moch, J.A.M. Vermaseren and A. Vogt, Nucl. Phys. B **688** (2004) 101 [hep-ph/0403192];
A. Vogt, S. Moch and J.A.M. Vermaseren, Nucl. Phys. B **691** (2004) 129 [hep-ph/0404111].
- [4] A.M. Cooper-Sarkar, arXiv:0707.1593 [hep-ph].
- [5] A. Djouadi and S. Ferrag, Phys. Lett. B **586** (2004) 345 [hep-ph/0310209].
- [6] A.D. Martin, W.J. Stirling, R.S. Thorne and G. Watt, Phys. Lett. B **652** (2007) 292 [arXiv:0706.0459 [hep-ph]].
- [7] S. Alekhin, K. Melnikov and F. Petriello, Phys. Rev. D **74** (2006) 054033 [hep-ph/0606237].
- [8] R.S. Thorne, Phys. Rev. D **73**, 054019 (2006) [hep-ph/0601245].
- [9] W.K. Tung *et al.*, JHEP **0702**, 053 (2007) [hep-ph/0611254].
- [10] P.D. Thompson, J. Phys. G **34**, N177 (2007) [hep-ph/0703103].

- [11] H.L. Lai *et al.*, JHEP **0704** (2007) 089 [hep-ph/0702268].
- [12] J. Pumplin, H.L. Lai and W.K. Tung, Phys. Rev. D **75** (2007) 054029 [hep-ph/0701220].
- [13] J. Blümlein, H. Böttcher and A. Guffanti, Nucl. Phys. B **774** (2007) 182 [hep-ph/0607200].
- [14] J. Blümlein, arXiv:0706.2430 [hep-ph].
- [15] C. Glasman for the H1 and ZEUS Collaborations, arXiv:0709.4426 [hep-ex].
- [16] P. Pétróff for the CDF and D0 Collaborations, these proceedings.
- [17] H1 and ZEUS Collaborations, report no. H1prelim-06-142 and ZEUS-prel-06-022 prepared for ICHEP 06, https://www-h1.desy.de/publications/H1preliminary.short_list.html
- [18] R.S. Thorne, hep-ph/0511351.
- [19] S. Forte, G. Altarelli and R.D. Ball, hep-ph/0606323.
- [20] C.D. White and R.S. Thorne, Phys. Rev. D **75** (2007) 034005 [hep-ph/0611204].
- [21] M. Ciafaloni, D. Colferai, G.P. Salam and A.M. Stasto, JHEP **0708** (2007) 046 [arXiv:0707.1453 [hep-ph]].
- [22] E. Iancu, hep-ph/0608086.
- [23] H. Kowalski, L. Motyka and G. Watt, Phys. Rev. D **74**, 074016 (2006) [hep-ph/0606272].
- [24] K.J. Golec-Biernat and S. Sapeta, Phys. Rev. D **74** (2006) 054032 [hep-ph/0607276].
- [25] G. Soyez, arXiv:0705.3672 [hep-ph].
- [26] E. Avsar and G. Gustafson, JHEP **0704** (2007) 067 [hep-ph/0702087].
- [27] M. Albrow *et al.*, CERN-CMS-NOTE-2007-002.
- [28] R. Venugopalan, arXiv:0707.1867 [hep-ph].
- [29] J. Bartels, K.J. Golec-Biernat and K. Peters, Eur. Phys. J. C **17** (2000) 121 [hep-ph/0003042].
- [30] A. Aktas *et al.* [H1 Collaboration], Eur. Phys. J. C **48** (2006) 715 [hep-ex/0606004].
- [31] ZEUS Collaboration, Abstract 63 submitted to EPS07, Manchester, England, 19–25 Jul 2007, ZEUS-prel-06-024.
- [32] K.J. Golec-Biernat and M. Wüsthoff, Phys. Rev. D **60** (1999) 114023 [hep-ph/9903358].
- [33] J.R. Forshaw, R. Sandapen and G. Shaw, JHEP **0611** (2006) 025 [hep-ph/0608161].
- [34] M. Diehl, Eur. Phys. J. C **25** (2002) 223, Erratum *ibid.* C **31** (2003) 277 [hep-ph/0205208].
- [35] K. Kumerički, D. Müller and K. Passek-Kumerički, hep-ph/0703179.
- [36] L. Frankfurt, M. Strikman and C. Weiss, Phys. Rev. D **69** (2004) 114010 [hep-ph/0311231].
- [37] K. Goulianos, hep-ph/0407035.
- [38] A.A. Affolder *et al.* [CDF Collaboration], Phys. Rev. Lett. **84** (2000) 5043; P. Newman, talk at the Workshop on HERA and the LHC, DESY, 12–16 March 2007.
- [39] J.C. Collins, J. Phys. G **28** (2002) 1069 [hep-ph/0107252].
- [40] M.G. Albrow *et al.*, Letter of Intent CERN-LHCC-2005-025.
- [41] K. Goulianos, arXiv:0707.1055 [hep-ex].
- [42] B.E. Cox *et al.*, Eur. Phys. J. C **45** (2006) 401 [hep-ph/0505240]; M. Taševsky, talk at the the Workshop on HERA and the LHC, CERN, 6–9 June 2006.
- [43] B.E. Cox, F.K. Loebinger and A.D. Pilkington, arXiv:0709.3035 [hep-ph].
- [44] S. Heinemeyer *et al.*, arXiv:0708.3052 [hep-ph].